Improving Water Spray Efficacy for Fire Suppression via CO_2 Addition at High Pressures and Low Temperatures: Evidence for CO_2 Clathrate Hydrate Formation

Shawn E. Hunter

Department of Chemical Engineering, University of Michigan, Ann Arbor, Michigan 48109

Lixiong Li* and Doug Dierdorf

Applied Research Associates, Inc., 430 West 5th Street, Suite 700, Panama City, Florida 32401

Timothy Armendinger

Air Force Research Laboratory, Tyndall Air Force Base, Florida 32403

This paper describes a technique for achieving a compact aqueous spray that incorporates CO_2 into the spray at low temperatures ($T < 10$ °C) and high pressures ($P > 10$ MPa). A high-pressure spray apparatus was used to explore the effects of temperature (4−25 °C), nominal CO_2 mole fraction (0−0.12), in-line filter pore size (0.5−7 μm), and additives on the high-pressure (12−19 MPa) water spray patterns. Divergence of the high-pressure H_2O-CO_2 spray was significantly reduced at low temperatures, with addition of sodium lauryl sulfate or aqueous film-forming foam (AFFF), and with a small-pore-size (0.5 μm) filter. The observed trends, based on digital images, can be explained by the formation of CO_2 clathrate hydrate within the continuous-flow system. The concepts discussed herein may be applied to conventional H_2O/AFFF fire-suppression systems, where the introduction of CO_2 as a foaming agent can increase fire-suppression efficacy.

1. Introduction

Recent efforts at Air Force Research Laboratory—AFRL (Tyndall Air Force Base, Florida) have led to the development and successful deployment of a novel high-pressure (10 MPa) water/aqueous film-forming foam (AFFF) spray delivery system for fire suppression.[1] Full-scale fuel fire tests showed that the high-pressure system extinguished the fuel fire in only 20 s with a water consumption of 50 L, whereas the conventional low-pressure (1.4 MPa) system was unable to extinguish the fire in 120 s with a water consumption of 680 L. The enhanced effectiveness of the high-pressure system was attributed to an increased degree of foam expansion resulting from increased turbulence associated with the high-pressure spray.

Further research and development efforts explored the idea of introducing a gas into the high-pressure H_2O/AFFF system to act as a foam-expanding agent. The performance of the high-pressure H_2O/AFFF system was further improved when high-pressure CO_2 was added to the system. In this CO_2/H_2O/AFFF system, the test fire was extinguished in 15 s with a water consumption of 24 L. However, the introduction of CO_2 at ambient temperature reduced the water jet throw distance (distance from the nozzle tip to the point at which the water jet contacts the fire target) from 12.2 to 7.6 m, because of rapid expansion of CO_2 gas at the nozzle exit. These opposing effects resulting from the added CO_2 prompted an investigation into the development of a technique that enables gas delivery for increased foam expansion, while maintaining the throw distance of the original system. Such a technique would be of interest for widespread fire-suppression applications.

One technique for improving the throw distance of a high-pressure CO_2/H_2O/AFFF system may be to incorporate the CO_2 into the stream as a gas hydrate. Gas hydrates, also known as clathrate hydrates, are ice-like solid phases that form at high pressure and low temperature.[2] Consisting of roughly 15 mol % gas and 85 mol % water, gas hydrates offer tremendous potential for gas storage and have been explored recently for carbon sequestration[3−7] within the deep ocean and for natural gas[8] and hydrogen[9] storage and transportation. Formation of CO_2 hydrate particles within the high-pressure fire-suppression system, and ejection of those particles from the nozzle along with the H_2O/AFFF stream, may provide a more practical method of assimilating CO_2 into the spray. If dissociation of the CO_2 hydrate and expansion of the CO_2 gas do not occur to a significant extent until the spray reaches the fire, then CO_2 may be delivered in the H_2O/AFFF stream as a foam-forming agent without the detrimental effect on the throw distance observed in the ambient temperature CO_2/H_2O/AFFF system.

The stability of CO_2 hydrate is a strong function of pressure, as shown in Figure 1. For example, pressures > 1.4 MPa are required to form CO_2 hydrate at 1 °C, whereas pressures > 4.4 MPa are required at 10 °C. Hence, if operated at $T < 10$ °C, the high-pressure spray delivery system[1] will provide the thermodynamic conditions necessary for CO_2 hydrate formation.

The hydrate formation process is believed to be similar to the crystallization process, whereby ordered clusters of CO_2 and H_2O molecules arrange to form hydrate precursors.[11] Precursors that reach a stable nuclei size grow quickly to form hydrate crystals. However, the nucleation process is stochastic in nature,[12] and induction times have varied from a few seconds to several days.[13,14] The random nature of hydrate nucleation has presented significant difficulty in understanding the complex nucleation mechanism,[12] which is influenced by many factors,

* To whom correspondence concerning this article should be addressed. E-mail: lli@ara.com. Tel.: (850) 914-3188. Fax: (850) 914-3189.

10.1021/ie060530p CCC: $33.50
Published on Web 09/19/2006

REPORT DOCUMENTATION PAGE

Form Approved
OMB No. 0704-0188

PLEASE DO NOT RETURN YOUR FORM TO THE ABOVE ADDRESS.

1. REPORT DATE *(DD-MM-YYYY)*	2. REPORT TYPE	3. DATES COVERED *(From - To)*
05-10-2006	Journal Article POSTPRINT	15-12-2003 to 25-04-2005

4. TITLE AND SUBTITLE

Improving Water Spray Efficacy for Fire Suppression via CO2 Addition at High Pressures and Low Temperatures: Evidence for CO2 Clathrate Hydrate Formation

5a. CONTRACT NUMBER

F08637-03-C-6006

5b. GRANT NUMBER

5c. PROGRAM ELEMENT NUMBER

63851D

6. AUTHOR(S)

Hunter, Shawn E.; Li, Lixiong; Dierdorf, Doug; Armendinger, Timothy

5d. PROJECT NUMBER

OAFT

5e. TASK NUMBER

01

5f. WORK UNIT NUMBER

OAFT0179

7. PERFORMING ORGANIZATION NAME(S) AND ADDRESS(ES)

Applied Research Associates
139 Barnes Drive, Suite 2
Tyndall AFB FL 32403-5323

8. PERFORMING ORGANIZATION REPORT NUMBER

9. SPONSORING/MONITORING AGENCY NAME(S) AND ADDRESS(ES)

Air Force Research Laboratory
Materials and Manufacturing Directorate
139 Barnes Drive, Suite 2
Tyndall AFB, FL 32403-5323

10. SPONSOR/MONITOR'S ACRONYM(S)

AFRL/MLQL

11. SPONSOR/MONITOR'S REPORT NUMBER(S)

AFRL-ML-TY-TP-2005-4543

12. DISTRIBUTION/AVAILABILITY STATEMENT

Distribution Statement A: Approved for public release; distribution unlimited.

13. SUPPLEMENTARY NOTES

Document contains color images. Published in American Chemical Society's Ind. Eng. Chem. Res (2006), Vol 45, pp 7275-7286.

14. ABSTRACT

This paper describes a technique for achieving a compact aqueous spray that incorporates CO_2 into the spray at low temperatures (T < 10 °C) and high pressures (P > 10 MPa). A high-pressure spray apparatus was used to explore the effects of temperature (4-25 °C), nominal CO_2 mole fraction (0-0.12), in-line filter pore size (0.5-7 ím), and additives on the high-pressure (12-19 MPa) water spray patterns. Divergence of the high-pressure H_2O-CO_2 spray was significantly reduced at low temperatures, with addition of sodium lauryl sulfate or aqueous film-forming foam (AFFF), and with a small-pore-size (0.5 ím) filter. The observed trends, based on digital images, can be explained by the formation of CO_2 clathrate hydrate within the continuous-flow system. The concepts discussed herein may be applied to conventional H_2O/AFFF fire-suppression systems, where the introduction of CO_2 as a foaming agent can increase fire-suppression efficacy.

15. SUBJECT TERMS

high-pressure H2O-CO2 spray, CO2 clathrate hydrate, additives, and fire suppression

16. SECURITY CLASSIFICATION OF:			17. LIMITATION OF ABSTRACT	18. NUMBER OF PAGES	19a. NAME OF RESPONSIBLE PERSON
a. REPORT	b. ABSTRACT	c. THIS PAGE			Timothy Armendinger
U	U	U	UU	13	19b. TELEPHONE NUMBER *(Include area code)*

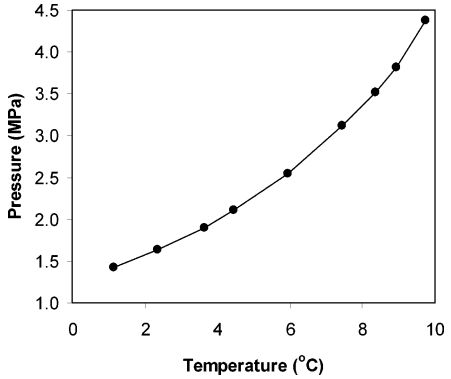

Figure 1. Three-phase (H_2O-rich liquid, CO_2 hydrate, and CO_2-rich vapor) equilibrium diagram for CO_2 hydrate. Data taken from Adisasmito et al.[10] Conditions for hydrate formation and stability are represented by the region on and above the curve. All experiments conducted herein were performed at pressures between 12 and 19 MPa, and hence, hydrate formation was possible in the low-temperature (T < 10 °C) runs.

including the thermal history[15] of the H_2O and the presence of additives.[16−18] Hence, the prediction of hydrate formation based on previously observed kinetics is unreliable, and experiments are required to investigate the formation of gas hydrate in a continuous system.

Motivated by the potential for spray-pattern improvement offered by the concept of CO_2 hydrate formation, we conducted an experimental study to examine the potential for incorporating CO_2 into an aqueous stream at low temperatures and high pressures. Previous experimental studies involving high-pressure H_2O-CO_2 flow systems at low temperatures have largely focused on the formation of CO_2 hydrate. Continuous systems have been applied recently to examine techniques for delivering CO_2 into the deep ocean for sequestration.[3−6] These flow systems have typically injected small amounts of one phase (liquid CO_2 or H_2O) into a large volume of the other phase. Much of the previous emphasis has been on simulating experimentally the release of liquid CO_2 drops[3,4] and CO_2 hydrate composite[5,6] into the deep ocean. Although these studies have examined the continuous formation of CO_2 hydrate, the delivery of hydrate particles into an ambient environment has not been examined previously. Thus, the present experimental study examines for the first time the ejection of a high-pressure, low-temperature H_2O-CO_2 stream into the surrounding atmosphere.

Effects of nominal CO_2 mole fraction (0−0.12), temperature (4−25 °C), additive, and mixing (in-line filter pore size 0.5−7 μm) on the ejected spray pattern were evaluated. Additive experiments were conducted with added potassium bicarbonate ($KHCO_3$), aqueous film-forming foam (AFFF), and sodium lauryl sulfate (SLS). $KHCO_3$ serves as the base compound for Purple K, a common dry chemical fire-suppression agent, and is, thus, present in many fire-suppression systems. AFFF is a fluorocarbon-based foaming agent routinely used by the Air Force for fire suppression and is, therefore, an additional relevant additive. SLS is a surfactant, and surfactants similar to SLS have been shown to promote hydrate formation in batch systems.[16,17] Data obtained from this study may be used to design more effective fire-fighting systems, which may appeal to a broad range of applications in the fire-fighting industry.

2. Experimental Section

2.1. Materials. Water used in this study was obtained from an in-house reverse osmosis (RO) system (Rainsoft model RSRO). Ice, produced from an in-house ice machine supplied with the RO water, was used to cool the feed water. Carbon dioxide was supplied from a liquid CO_2 cylinder (Airgas, Inc., 99.8%). Sodium lauryl sulfate (SLS) (Aldrich Chemical Co., Inc.) was used as received with the following composition: dodecyl sulfate, sodium salt (70%); tetradecyl sulfate, sodium salt (∼25%); and hexadecyl sulfate, sodium salt (∼5%). Potassium bicarbonate (99%, Aldrich Chemical Co., Inc.) and 3% AFFF solution (ANSUL Inc., 4210-01-139-4972, consisting of roughly 77−81% H_2O, 10% diethylene glycol butyl ether, 3−7% urea, 1−5% alkyl sulfate salts, 2% amphoteric fluoroalkylamide derivative, 0.1−1% triethanolamine, 0.1−1% perfluoroalkyl aulfonate salts, 0.05% tolyl triazole, and residual organic fluorochemicals) were also used as received.

2.2. Continuous-Flow System. Figure 2 depicts the H_2O-CO_2 flow system used in the hydrate-formation experiments. High-pressure (12 MPa < P < 19 MPa) water was delivered to the system using a high-pressure pump (Wagner, model 770). The pump operated at a constant head pressure, so that the H_2O flowrate decreased with increasing system pressure. The H_2O flowrate varied from 850 mL/min at 12 MPa to 730 mL/min at 19 MPa. The Wagner pump was equipped with a safety shut-off feature, which stopped flow at pressures above 17−19 MPa. The upper range of CO_2 mole fraction that could be examined was, hence, limited by this automatic shut-off feature. Liquid CO_2 was supplied to the system from a liquid CO_2 cylinder via a high-pressure pump and regulated with control software, both of which were obtained from a supercritical fluid extraction system (Thar Technologies, model SFE-500 mL). The flowrate of CO_2 was specified using the Thar ICM (version 2.5) control software and ranged from 0 to 200 mL/min. The liquid streams were combined using a $^1/_4$ in. Swagelok tee. Agitation of the resulting mixture and dispersion of the liquid CO_2 were achieved by passing the combined stream through an in-line stainless steel filter (Swagelok, P/N SS-2TF-7), containing a 7 or 0.5 μm pore

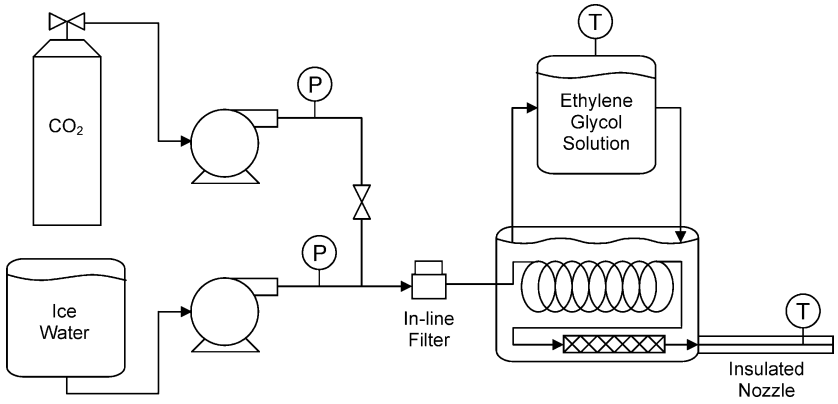

Figure 2. Experimental apparatus.

size sintered stainless steel filter element, which functioned similar to a static mixer. The filter pore size was 7 μm unless otherwise noted. The mixed stream was then sent through cooling coils and passed over a static mixer, both of which were submerged in a 40 L bath of 50% v/v aqueous ethylene glycol (antifreeze) solution held at roughly −3.0 °C and contained within a plastic cooler. The cooling coils consisted of a 72 in. long piece of $^1/_4$ in. tubing (0.035 in. w.t.) followed by a 196.7 in. long piece of $^1/_8$ in. tubing (0.020 in. w.t.), which fed into a 7.5 in. long segment of $^1/_2$ in. tubing (0.035 in. w.t.) connected to a second piece of $^1/_2$ in. tubing (8.0 in. long × 0.035 in. w.t.). The second piece of $^1/_2$ in. tubing contained the static mixer (Cole-Parmer, EW-04667-16, $^3/_8$ in. element diameter, $L/D = 1.04$, cut to 23 elements), which served to further increase the turbulence of the passing fluid mixture and, therefore, the dispersion of the CO_2 within the aqueous phase. Residence times of the H_2O-CO_2 mixture within the cooler were between 6 and 7 s. The temperature of the ethylene glycol solution was controlled using a circulating bath (Fisher Scientific, model 9501). After passing over the static mixer, the pressurized stream was then ejected from a 24 in. long section of 316 stainless steel capillary tubing ($^1/_8$ in. o.d. × 0.058 in. w.t.) into ambient (21 °C < T < 25 °C) air. The capillary tubing nozzle was mounted external to the cooler via a bulkhead reducing union sealed within a hole drilled in the cooler wall and was insulated with four layers of pipe insulation to minimize ambient heating of the cooled stream as it passed through the nozzle. The surface temperature of the nozzle, reported herein as the nozzle temperature and inferred as the temperature of the system during an experimental run, was measured by a Type E thermocouple fastened to the surface of the nozzle and underneath the first layer of insulation. The end of the thermocouple was located 2.5 cm from the end of the nozzle. Because of safety concerns, controllability of the ambient environment, and lighting requirements for photo imaging, the test apparatus was set up in a walk-in chemical fume hood with dimensions of 3 m wide by 3 m deep by 3 m high.

The pressure of the system, as measured by a pressure transducer located at the discharge port of the pump and reported herein as the system pressure, was recorded using the Thar ICM software. The system pressure was dictated by flow resistance offered by the capillary tubing and/or the filter element and could not be specified. Accumulation of solid material on the filter element resulted in small variations (±1.5 MPa) in the system pressure among experimental runs with identical CO_2 flowrates. The pressure was also recorded using a Bourdon tube pressure gauge located on the high-pressure water supply line. This pressure was typically within 0.3 MPa of the system pressure and was used to calibrate the H_2O flowrate delivered by the high-pressure water pump. For a given set of operating conditions, the system pressure increased and the H_2O flowrate decreased as the CO_2 flowrate increased.

2.3. Flow System Operation. The water feed was prepared by filling the water pump feed reservoir with RO water and ice. A plastic cooler was also filled with water and ice and was used as a backup feed reservoir for refilling the pump reservoir. A sufficient amount of ice was mixed in with the RO water to form an ice−water slurry (~0 °C). Additional ice was added to the pump feed reservoir, as necessary during the run, to maintain the presence of solid ice and a temperature near 0 °C in the feed reservoir. When required, additives were next added to each reservoir at the specified concentration, and the resulting solutions were thoroughly mixed. After the temperature of the circulating bath had reached the desired set point, the H_2O pump was turned on and the nozzle temperature was allowed to achieve thermal equilibrium. When the nozzle temperature reached steady state, the liquid-CO_2 pump was turned on. To prevent backflow of H_2O into the CO_2 supply line, a two-way straight ball valve was installed in the CO_2 line to allow pressure to build in the line before introducing the CO_2 stream into the H_2O stream. This valve was opened only after the CO_2 pump pressure was greater than the water supply line pressure. The system typically reached steady-state flow conditions after roughly 20 s of opening the valve and introducing the CO_2 stream. System conditions (nozzle temperature, pressure, and flowrate) were recorded only after the system had achieved a steady state and did not significantly deviate from the recorded values during the experiment. Several images of the steady-state spray at the given nozzle temperature, system pressure, filter pore size, additive concentration, and nominal CO_2 mole fraction were then captured using a digital camera. In some experiments, water-collection tests were also performed, as described below. After several (~5) images of the spray were captured, the CO_2 flow was increased to the next desired flowrate, and the procedure was repeated until all desired CO_2 flows were examined.

At a circulating bath temperature setting of −3.0 °C, the nozzle temperature with H_2O-only flow was typically 3−5 °C. With CO_2 flowing, however, the nozzle temperature increased, which suggested that the CO_2 was not adequately cooled before mixing with the H_2O. Placing a thermocouple at a tee in the CO_2 line upstream of the H_2O-CO_2 mixing point revealed that the CO_2 was entering the system at near-ambient temperature. Although the system pressure was always sufficiently high[7] (>5.5 MPa) to prevent boiling of the liquid CO_2 in the line, thermal effects were evident in some runs. For higher CO_2 flowrate runs (≥50 g/min), the final temperature after several minutes of run time was greater (~1 °C) than the initial temperature. After acquiring images under these conditions, the CO_2 flow was reduced to and held at 5 g/min for several minutes before increasing the CO_2 flow to the next desired flowrate, so that the initial nozzle temperature was similarly low for each run.

2.4. Photo Documentation. To compare the effect of varying system conditions on the spray pattern, a visualization technique was implemented. For each set of conditions, photo images were recorded using a digital camera (Nikon COOLPIX 5700). To provide good contrast of the spray in the images, a 1.3 cm thick piece of high-density foam rubber was painted black and used as a background. The black background was supported using a ring stand, and the top of the background was pitched at a slightly forward angle (toward the camera) to minimize the amount of overhead light reflected off of the painted rubber surface. Images from the digital camera served as the primary data type for determining the effect of system conditions on the spray pattern. Images were recorded both with the camera flash off, which captured the overall spray pattern and which comprise the majority of the images presented herein, and with the flash on, which revealed more detailed images of individual liquid droplets or particles. These images were collectively assessed to determine the effect of different system conditions on the divergence and form of the spray pattern.

2.5. Water-Collection Tests. An additional technique for assessing the effect of system variables on the ejected spray is quantification of the throw distance. Because the throw distance of the system was much greater than the space available (~1.5 m) in the walk-in hood, direct measurement of the throw distance was not possible. However, the qualitative effect of

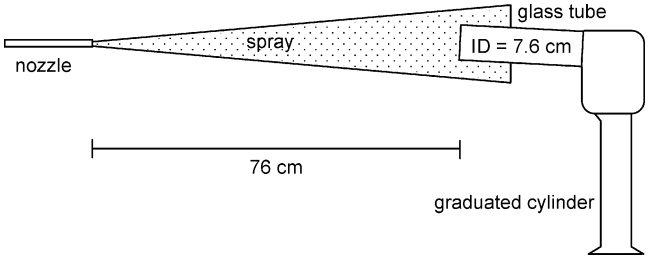

Figure 3. Schematic of water-collection test setup.

system variables on throw distance can be inferred by examining the compactness of the ejected spray. Therefore, a water-collection system was used to quantify the compactness of the ejected spray in some experiments. This system was used to determine the fraction of water passing through a constant cross-sectional area at a constant distance from the end of the nozzle. The water-collection test setup, depicted in Figure 3, consisted of a 7.6 cm diameter glass tube connected to a 5 L graduated cylinder. The cross-sectional area of the tube was smaller than that of a fully divergent spray and was, thus, appropriate for quantifying the transition in spray pattern from compact to divergent. The glass tube was placed 76 cm from the nozzle exit and directly in front of the ejected spray. A slight pitching of the glass tube prevented backsplash and directed all spray entering the tube into the graduated cylinder for collection. In a typical water-collection test, roughly 1−2 L of water was collected in the graduated cylinder under steady-state flow conditions. For these experiments, the fraction f of water collected was calculated as the volume of water collected in the graduated cylinder divided by the total volume of water delivered from the nozzle (based on the water pump flowrate and the time of the test). The value of f was, therefore, equal to unity for a compact stream and decreased as the spray diverged outside of the collection area. Thus, comparing values of f for different conditions provides a means of quantifying the effects of those conditions on the compactness of the ejected stream.

2.6. Presence of CO_2 Clathrate Hydrate. Identification and quantification of CO_2 hydrate particles, present in small quantities relative to the liquid phase and in a continuous-flow system, is not trivial. Several studies have incorporated visualization techniques to positively identify the formation of gas hydrates, in both batch[14,19] and continuous systems.[5,6] In these previous studies, significant amounts of gas hydrate were formed, thereby permitting the use of visualization to confirm the presence of hydrate. In the present study, macroscopic amounts of a solid material that could be positively identified as CO_2 hydrate were not observed in the ejected spray or in the spray images. In some cases, visualization images captured with the camera flash on revealed "dots" in the spray, the concentration of which was dependent on system conditions. Some of these dots were simply liquid droplets; others may have contained CO_2 hydrate, as discussed in Section 3.7. However, visual confirmation of these dots alone does not provide unambiguous evidence for hydrate formation.

Other techniques to confirm hydrate formation, which have been successfully applied to unsteady-state batch systems, have relied on measuring the amount of gas added to a closed chamber or have related fluctuations in pressure and temperature to hydrate formation within the system.[17,19] For a steady-state continuous flow system, however, no simple gas consumption or system variable fluctuation analogues exist.

Analytical techniques such as Raman spectroscopy[20] and differential scanning calorimetry[21,22] have been applied to confirm the presence of gas hydrate. Additionally, imaging techniques, including scanning electron microscopy,[23] nuclear magnetic resonance,[24,25] and X-ray tomography,[26] and diffraction techniques, including X-ray[27] and neutron[28,29] diffraction, have examined the structure of gas hydrates and have been used to study their formation and growth. Application of these techniques to the present work would require collection of the ejected spray, isolation of hydrate-containing particles from the collected spray, and preservation of those particles at temperatures below or pressures above their dissociation point for subsequent analysis. In the present experiments, the high-pressure spray was ejected into the ambient environment, and solid particles were not observed in the liquid collected during water-collection tests. While it may be possible to collect and isolate hydrate formed within the present system, the implementation of these advanced spectroscopic, imaging, or diffraction techniques to positively identify the formation of CO_2 hydrate within the system was not within the scope of this preliminary study. The focus, rather, was to identify a practical technique for improving the spray pattern of a high-pressure H_2O-CO_2 spray, which was motivated by the potential in situ formation of CO_2 hydrate. Whereas evidence consistent with hydrate formation is presented here, future studies incorporating one or more of the aforementioned analytical techniques could provide unambiguous evidence for the continuous formation of CO_2 hydrate within similar flow systems.

Table 1. Summary of Experimental Runs

data set	additive	filter pore size (μm)	system pressure[a] (MPa)	nozzle temp (°C)	$x_{CO_2}^*$
1	none	7	12−19	20−23	0−0.12
2	none	7	14−17	4−7	0−0.03
3	none	0.5	13−18	4−6	0−0.10
4	100 ppm of SLS	7	15−19	5−6	0−0.10
5	100 ppm of $KHCO_3$	7	14−15	4−5	0−0.03
6	100 ppm of AFFF	7	12−18	5−6	0−0.10
7	3300 ppm of AFFF	7	13−17	5−8	0−0.05

[a] In data sets 2−7, the pressure required for hydrate formation was <4 MPa.

3. Results and Discussion

Table 1 presents a summary of the conditions examined in this study. For each data set, images were acquired for between 4 and 11 different values of the nominal CO_2 mole fraction $x_{CO_2}^*$. Here, $x_{CO_2}^*$ is calculated as

$$x_{CO_2}^* = \frac{\dot{n}_{CO_2}}{\dot{n}_{CO_2} + \dot{n}_{H_2O}}$$

where $\dot{n}_{CO_2}$ and $\dot{n}_{H_2O}$ are the molar flowrates of CO_2 and H_2O, respectively, delivered by the high-pressure CO_2 and H_2O pumps. Values of $x_{CO_2}^*$ were typically 0.01−0.03 and were, in some cases, lower than the solubility x_{CO_2} of CO_2 in H_2O. For example, $x_{CO_2} = 0.025$ mole fraction at 6 °C and 12 MPa.[30] In the present system, a filter served to mix the H_2O-CO_2 stream. We speculate that the liquid CO_2 stream was broken into small drops as it passed through the 0.5 or 7 μm pore size filter and into the H_2O stream. Hence, our system was not homogeneous, and the values of reported $x_{CO_2}^*$ in Table 1 do not reflect a homogeneous mole fraction of CO_2 in the system. Rather, the local CO_2 mole fraction near the dispersed liquid CO_2 drops was higher than $x_{CO_2}^*$, and H_2O near the CO_2 drops was supersaturated in CO_2.[31]

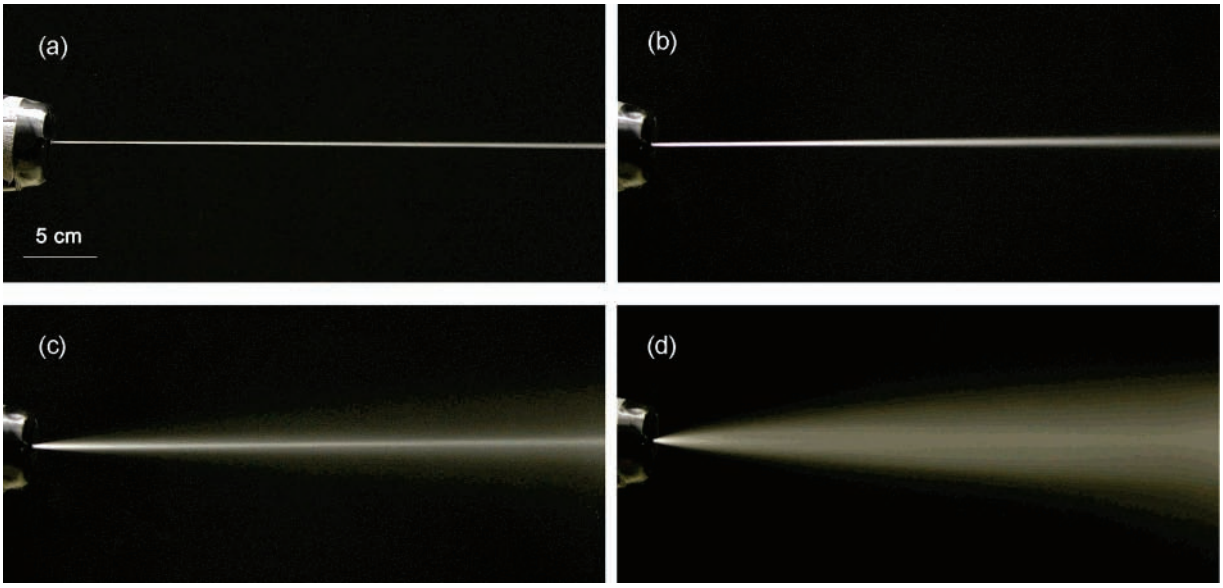

Figure 4. CO_2-H_2O spray pattern at ambient temperature: (a) $x_{CO_2}^* = 0$, $T = 25$ °C, $P = 11.7$ MPa; (b) $x_{CO_2}^* = 0.012$, $T = 23$ °C, $P = 12.6$ MPa; (c) $x_{CO_2}^* = 0.014$, $T = 23$ °C, $P = 12.6$ MPa; (d) $x_{CO_2}^* = 0.017$, $T = 24$ °C, $P = 13.5$ MPa.

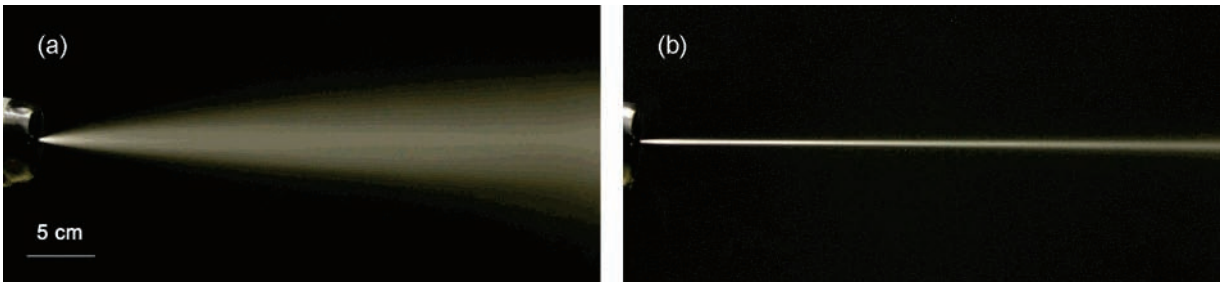

Figure 5. Effect of temperature on CO_2-H_2O spray pattern: (a) $T = 24$ °C, $P = 13.5$ MPa, $x_{CO_2}^* = 0.017$; (b) $T = 7$ °C, $P = 14.9$ MPa, $x_{CO_2}^* = 0.018$.

During the study, several hundred images were recorded. In the following discussion, which provides interpretation of these images, only representative images are shown. In these experiments, the CO_2 flowrate, rather than $x_{CO_2}^*$, was specified. Because of slight variations in the system pressure and resulting variations in the H_2O flowrate for different experimental runs at the same CO_2 flowrate, $x_{CO_2}^*$ varied slightly between runs with identical CO_2 flowrates. These differences are sufficiently small such that any conclusions reached by comparing runs at similar but not identical $x_{CO_2}^*$ or system pressure will be independent of the slight variation in those quantities.

3.1. Effect of Nominal CO_2 Mole Fraction on Spray Pattern. Baseline experiments at room temperature were conducted to observe the effect of increasing the nominal CO_2 mole fraction on the spray pattern. Figure 4 shows images obtained during these experiments. At low $x_{CO_2}^*$, the spray appeared as a compact jet and diverged only slightly as $x_{CO_2}^*$ increased from 0 to 0.012 (Figure 4 parts a and b). At a nominal CO_2 mole fraction of 0.014 (Figure 4c), however, a small amount of the flow expanded rapidly upon exiting the nozzle, and the spray showed signs of significant divergence. Increasing $x_{CO_2}^*$ to just 0.017 led to the development of a fully divergent spray, as shown in Figure 4d. Hence, increasing the nominal CO_2 mole fraction leads to a transition in the spray pattern from a compact liquid jet to a divergent spray.

3.2. Effect of Temperature on Spray Pattern. Experiments at low nozzle temperatures (4−7 °C) were conducted to elucidate the effect of temperature on the spray pattern. As in the ambient temperature experiments, increasing the nominal CO_2 mole fraction to sufficiently high values induced divergence in the spray pattern. However, at these reduced temperatures, the transition from compact jet to divergent spray occurred at higher $x_{CO_2}^*$. Figure 5 shows that the spray was divergent at ambient temperature and $x_{CO_2}^* = 0.017$. At a nozzle temperature of 7 °C (and $x_{CO_2}^* = 0.018$), however, the spray was a compact jet and did not diverge to a great extent within the distance observed in the spray images. These results demonstrate that a significant reduction in the divergence of high-pressure H_2O-CO_2 sprays at ambient temperature can be achieved by lowering the system temperature to within several degrees of the freezing point.

The reduction in spray divergence observed at low temperatures could be the simple result of the reduced temperature on the expansion of liquid CO_2 in the system. Liquid CO_2 may not have dissolved completely in the aqueous phase because of insufficient mixing or solubility[30] limitations. Undissolved liquid CO_2 pockets at higher temperatures are expected to vaporize more quickly and cause greater spray divergence than at lower temperatures. Hence, the decrease in spray divergence at low temperatures can be explained by a lower rate of liquid CO_2 vaporization at the nozzle exit.

A second explanation of the spray divergence reduction is that CO_2 hydrate formed in the system at lower temperatures. At temperatures below 10 °C and pressures above 4.5 MPa, CO_2 hydrate formation is possible in H_2O-CO_2 systems.[32] In the low-temperature runs discussed here, the pressure was at least 12 MPa, liquid CO_2 was dispersed into the H_2O stream, and, hence, hydrate formation was possible. CO_2 hydrate may have formed at any H_2O-CO_2 interface, one example being the surface of liquid CO_2 drops. CO_2 hydrate formation

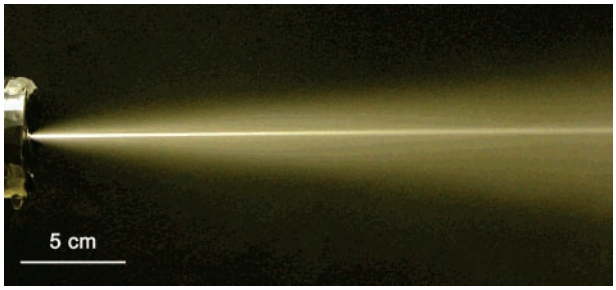

Figure 6. CO_2-H_2O spray pattern without filter: $x_{CO_2}^* = 0.017$, $T = 4$ °C, $P = 9.1$ MPa.

effectively serves as a sink for CO_2, as CO_2 required to form the hydrate must be removed directly from the liquid CO_2 or aqueous phases. Furthermore, the isolation of liquid CO_2 within hydrate-covered CO_2 drops serves as another mechanism by which liquid CO_2 is functionally reduced within the flow. Sequestering CO_2 in hydrate crystals and in hydrate-covered CO_2 drops would leave less CO_2 available in the flow to expand immediately after exiting the nozzle, provided that the dissociation of CO_2 hydrate is slower than the expansion of liquid or gaseous CO_2. Thus, the formation of hydrate within the system would lead to a less-divergent spray and, hence, account for the observed spray behavior. This reduction in spray divergence is expected to occur for any run in which a significant amount of CO_2 hydrate formed.

3.3. Formation of CO_2 Hydrate. CO_2 hydrate is a nonstoichiometric compound, with equilibrium hydrate phase CO_2 mole fractions being estimated as low as 0.115.[31] In the present experiments, $x_{CO_2}^*$ was typically well below this value. However, gas hydrate tends to form at the interface of the water and guest phases,[14,33] and hydrate formation has been observed previously on the surface of liquid CO_2 drops in H_2O-CO_2 mixtures.[34,35] Kinetic modeling estimates have suggested that the formation of hydrate on the surface of liquid CO_2 drops in high-pressure, low-temperature water is rapid, with the drops being completely covered by hydrate in <2 s, which is less than the residence time in the present experimental apparatus, at $T < 10$ °C and $P > 4.5$ MPa.[36,37] Furthermore, because hydrate formation is a local phenomenon, and because the aqueous interphase surrounding H_2O-dispersed liquid CO_2 droplets is supersaturated with CO_2,[31] hydrate formation on liquid CO_2 droplets is likely to occur even when the bulk concentration of CO_2 in the H_2O is well below the solubility of CO_2.[31] Thus, any hydrate that formed in the present experiments most likely formed on the surface of liquid CO_2 droplets present in the system.

3.4. Effect of Filter Pore Size on Spray Pattern. Background experiments revealed that a filter, placed between the stream combination tee and the cooler, was necessary for achieving a uniform H_2O-CO_2 spray at all temperatures. Omission of the filter led to a spray pattern that consisted of a compact liquid jet centered within a divergent gaseous spray, as shown in Figure 6. In addition to the lack of homogeneity of the spray pattern, intermittent bursts of gas present under these conditions suggested that the H_2O-CO_2 flow was poorly mixed in the absence of a filter.

To examine the effect of filter pore size on the spray pattern at low temperature, we conducted experiments using a 0.5 μm filter element (data set 3) for comparison to the 7 μm filter element experiments (data set 2). Figure 7 provides representative images that demonstrate the effect of filter pore size on the H_2O-CO_2 stream. Parts a and b of Figure 7 display the spray pattern at $x_{CO_2}^* = 0.017-0.018$ observed with each filter. With a pore size of 7 μm, the spray exhibited a small amount of gas dissociating from the stream, and there was small but clear divergence throughout the spray. With the 0.5 μm filter, however, there was no visible gas in the spray, and relatively little divergence. The effect of filter pore size is dramatically illustrated in parts c and d of Figure 7, which show the system at $x_{CO_2}^* = 0.024-0.026$. Here, the spray with the 0.5 μm filter was clearly less gaseous than the spray with the 7 μm filter. The results of these experiments clearly illustrate the sensitivity of the spray pattern to the filter pore size.

The improvement in spray pattern that occurred first by including a filter in the system, and then by reducing the filter pore size, was likely due to increased dispersion of the liquid CO_2 within the H_2O stream. Passing the H_2O-CO_2 mixture through a micron-sized filter likely led to the formation of finely dispersed liquid CO_2 particles. The formation of these particles

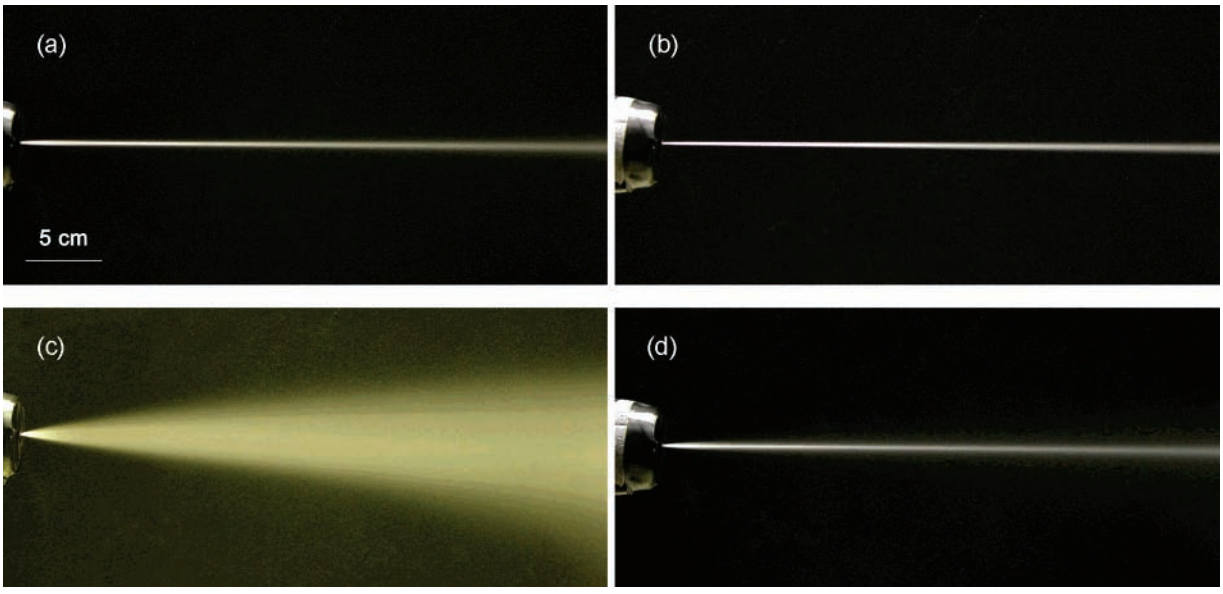

Figure 7. Effect of filter pore size on CO_2-H_2O spray pattern: (a) 7 μm filter, $x_{CO_2}^* = 0.018$, $T = 5$ °C, $P = 15.0$ MPa, $f = 1$; (b) 0.5 μm filter, $x_{CO_2}^* = 0.017$, $T = 5$ °C, $P = 13.6$ MPa, $f = 1$; (c) 7 μm filter, $x_{CO_2}^* = 0.026$, $T = 5$ °C, $P = 16.8$ MPa, $f = 0.31$; (d) 0.5 μm filter, $x_{CO_2}^* = 0.024$, $T = 6$ °C, $P = 14.4$ MPa, $f = 1$.

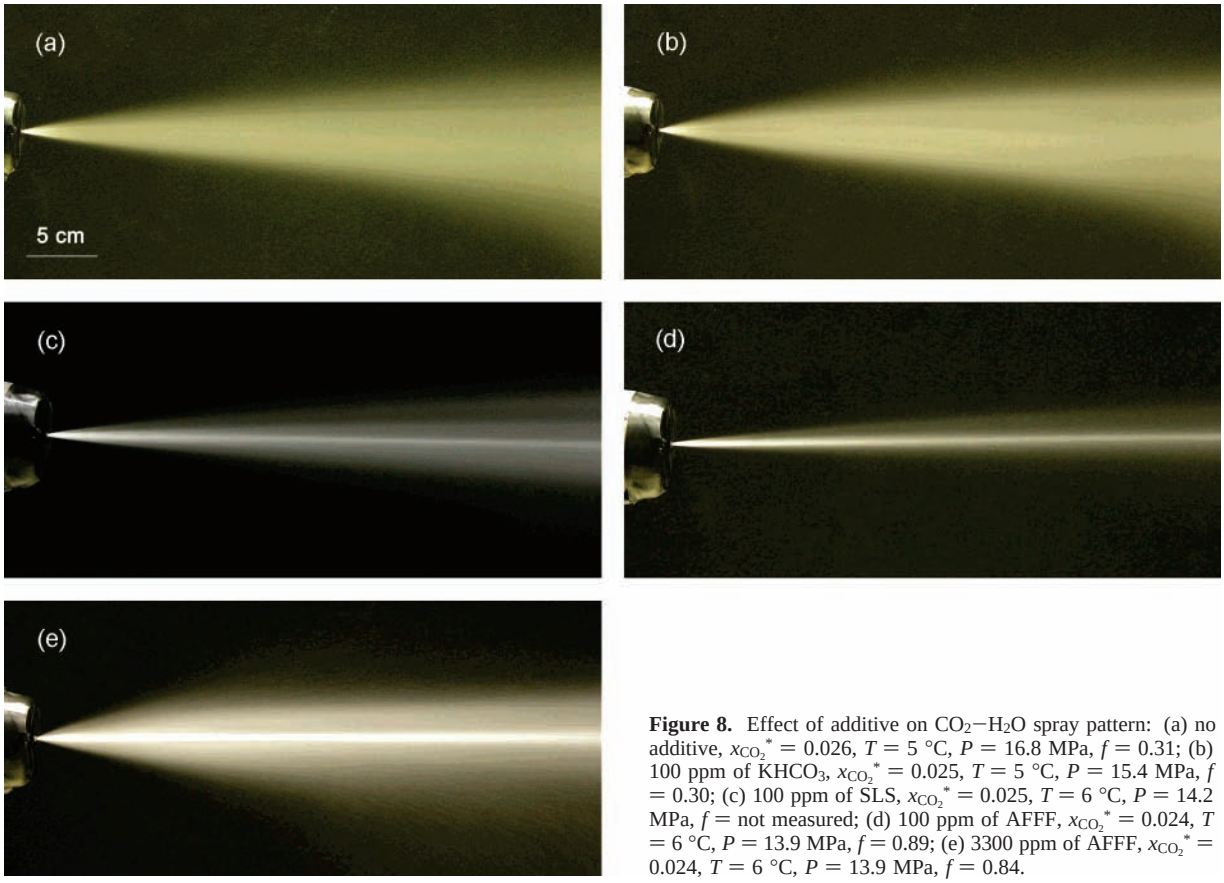

Figure 8. Effect of additive on CO_2-H_2O spray pattern: (a) no additive, $x_{CO_2}^* = 0.026$, $T = 5$ °C, $P = 16.8$ MPa, $f = 0.31$; (b) 100 ppm of $KHCO_3$, $x_{CO_2}^* = 0.025$, $T = 5$ °C, $P = 15.4$ MPa, $f = 0.30$; (c) 100 ppm of SLS, $x_{CO_2}^* = 0.025$, $T = 6$ °C, $P = 14.2$ MPa, $f =$ not measured; (d) 100 ppm of AFFF, $x_{CO_2}^* = 0.024$, $T = 6$ °C, $P = 13.9$ MPa, $f = 0.89$; (e) 3300 ppm of AFFF, $x_{CO_2}^* = 0.024$, $T = 6$ °C, $P = 13.9$ MPa, $f = 0.84$.

would have eliminated any large liquid CO_2 pockets that existed within the flow. This explanation is consistent with the lack of intermittent gas bursts that was observed for all filter-equipped runs. Additionally, reducing the filter pore size would lead to smaller liquid CO_2 particles. The resulting increase in H_2O-CO_2 contact area would both promote enhanced dissolution of the CO_2 into the H_2O and provide greater opportunity for CO_2 hydrate formation. The occurrence of either phenomenon would decrease the amount of liquid CO_2 present in the H_2O-CO_2 stream and leave less liquid CO_2 available at the nozzle exit to immediately vaporize and cause spray divergence. Hence, these results suggest that increasing the dispersion of CO_2 within the H_2O flow can decrease the amount of undissolved CO_2 present at the nozzle, and offer an additional method for reducing the divergence of high-pressure H_2O-CO_2 sprays.

3.5. Effect of Additives on Spray Pattern. Experimental conditions for runs performed with added SLS, $KHCO_3$, and AFFF (data sets 4−7) are listed in Table 1. Figure 8 illustrates the effect of additives at low temperatures. At $x_{CO_2}^* = 0.026$ without additive, the spray was divergent, as shown in Figure 8a. The addition of $KHCO_3$ at 100 ppm (Figure 8b) had no significant effect on the spray pattern at these conditions. However, the addition of 100 ppm of SLS led to a reduction in divergence, as shown in Figure 8c. Further, the addition of 100 ppm of AFFF (Figure 8d) also led to a less-divergent spray, which was more compact than that obtained with the 100 ppm of SLS. Increasing the AFFF concentration to 3300 ppm (Figure 8e) led to an apparent increase in spray divergence when compared with the 100 ppm run.

The influence of SLS, AFFF, and $KHCO_3$ on the spray pattern can be summarized as follows. The addition of 100 ppm of SLS and 100 ppm of AFFF led to a reduction in spray divergence when compared to the spray without additive (up to $x_{CO_2} = 0.03$). In contrast, the addition of $KHCO_3$ had no effect on the spray pattern over all CO_2 mole fractions examined. Further, the addition of 3300 ppm of AFFF resulted in a foamy spray that exhibited apparent divergence similar to that without additive. However, the presence of a significant amount of foam in the spray likely revealed a wider spray path than was visible in the absence of foam, and so the exact effect of large quantities of AFFF on the spray cannot be determined from this visual evidence alone.

These results suggest that additives can be used in a high-pressure H_2O-CO_2 flow system to influence the ejected stream's spray pattern. Although $KHCO_3$ did not affect the spray pattern, the addition of both SLS and AFFF led to a reduction in divergence of the spray. This reduction may have been due to the formation of hydrate in the system. In the case of SLS, the formation of CO_2 hydrate is consistent with previous studies,[16,17] which indicated that hydrate formation is promoted by surfactants similar to SLS. SLS may have enhanced hydrate formation by increasing hydrate stability (decreasing the pressure or increasing the temperature of dissociation[38]) or promoting reproducible induction times.[16] No previous reports have addressed the addition of AFFF as a hydrate promoter. In our experiments, the role of added AFFF may also be to increase the rate of hydrate formation, due to it also being a surfactant. Another explanation of the observed reduction in spray divergence with AFFF is that CO_2 served as a foaming agent for the AFFF and was, hence, trapped in foam that formed as the stream was ejected from the nozzle. This occurrence also would have reduced the amount of CO_2 available to expand freely in the ejected stream, leading to a less-divergent spray. An additional explanation for the improvement in spray pattern observed with SLS or AFFF is that the addition of these surfactants increased the stability of the ejected spray. The addition of selected

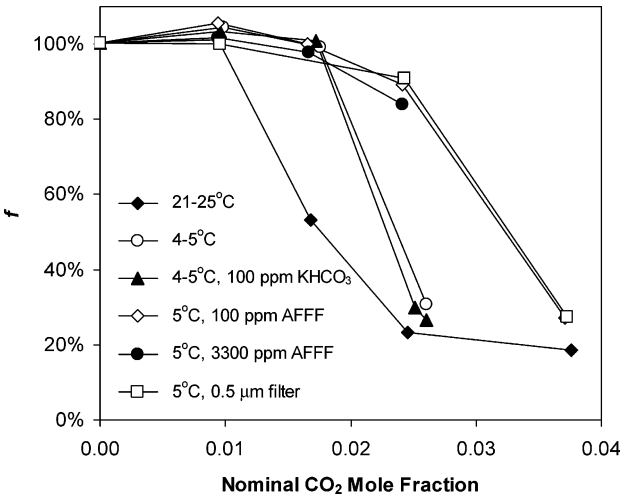

Figure 9. Effect of nominal CO_2 mole fraction and system conditions on *f*, the fraction of water collected.

surfactants has been shown to increase the stability of ejected aqueous sprays.[39,40] Although the addition of surfactants leads to reduced surface tension, surfactants may act to hinder instability growth or increase the maximum sustainable amplitude of instability, thereby reducing the tendency of the ejected spray to break up.[40]

3.6. Effect of System Conditions on Spray Compactness. Water-collection tests were conducted to quantify the compactness of spray and to assess the effect of system conditions on throw distance. These tests were performed under the following conditions: (a) ambient temperature (21−25 °C), (b) 4−5 °C, (c) 4−5 °C with 100 ppm of $KHCO_3$, (d) 5 °C with 100 ppm of AFFF, (e) 5 °C with 3300 ppm of AFFF, and (f) 5 °C with 0.5 μm filter pore size.

Figure 9 displays the results of the water-collection tests. Considering the ambient temperature (21−25 °C) run, all of the ejected water was recovered at low $x_{CO_2}^*$, and *f* was equal to 1.0. As $x_{CO_2}^*$ increased from 0.009 to 0.017 at this temperature, *f* decreased from 1.0 to 0.53. Increasing $x_{CO_2}^*$ to 0.025 led to a further reduction in *f* to 0.23. However, increasing $x_{CO_2}^*$ above 0.025 led to no significant change in *f*, up to $x_{CO_2}^* = 0.10$. Hence, these data illustrate quantitatively the transition in spray pattern from compact liquid jet to divergent spray as $x_{CO_2}^*$ is increased. Further, the data imply that high throw distances were achieved at ambient temperature and $x_{CO_2}^* < 0.009$, and that the throw distance was significantly shortened by increasing $x_{CO_2}^*$ above 0.009. Additionally, the data at high $x_{CO_2}^*$ indicate that the divergent spray, once fully established, is independent of the amount of CO_2 present.

Figure 9 further demonstrates the effect of varying system conditions on the stability of the ejected spray. Lowering the temperature from ambient to 4−5 °C led to an increase in the amount of CO_2 that could be added to the system before *f* decreased below unity (from $x_{CO_2}^* = 0.009$ to $x_{CO_2}^* = 0.017$). This increase implies that a high throw distance can be maintained at greater $x_{CO_2}^*$ by operating at low temperatures. Adding 100 ppm of $KHCO_3$, however, did not affect the *f* profile at 4−5 °C and, thus, had no effect on the throw distance. Conversely, the addition of AFFF and the decrease in filter pore size did lead to a more stable stream and higher values of *f* for nominal CO_2 mole fractions up to $x_{CO_2}^* = 0.025$. This improvement is most clearly observed at $x_{CO_2}^* = 0.025$, where *f* increased from 0.30 for the 4−5 °C run without additive to 0.84, 0.89, and 0.91 for the 3300 ppm of AFFF, 100 ppm of AFFF, and 0.5 μm filter runs, respectively. Hence, a high throw distance was maintained at nominal CO_2 mole fractions up to $x_{CO_2}^* = 0.025$ by using AFFF as an additive or by reducing the filter pore size.

The results of these tests imply that some techniques can be applied to preserve high distances in high-pressure H_2O sprays with added CO_2. The application of low temperature, the addition of AFFF, and the use of small filter pore size all led to an increase in the maximum amount of CO_2 that could be added to the spray before significantly reducing the throw distance. These results are consistent with the spray pattern results shown in the digital images.

Figure 9 also demonstrates that the addition of 3300 ppm of AFFF to the spray did lead to a reduction in spray divergence, despite the apparent increase in divergence observed in Figure 8. At $x_{CO_2}^* = 0.025$, *f* was much higher in the 3300 ppm AFFF run (0.89) than in the low-temperature run without additive (0.30), and hence, the spray was less divergent in the presence of 3300 ppm of AFFF. Thus, AFFF is an effective additive for achieving an improved spray pattern over the concentration range of 100−3300 ppm.

3.7. Observation of Dots in the Spray. Small "dots" were routinely observed in spray images captured with the camera flash on. Figure 10 (parts a−e) provides a comparison of these dots at $x_{CO_2}^* = 0.024-0.026$ and varying system conditions. At ambient temperature (Figure 10a), a small number of dots appeared within and surrounding the largely gaseous spray. At low temperatures without additive (Figure 10b), and with 100 ppm of $KHCO_3$ (Figure 10c), a small number of dots were also present in the spray but were more concentrated in the flow field because of the reduction in divergence observed at low temperatures when compared to ambient temperature. However, with 100 ppm of SLS (Figure 10d), the concentration of dots increased significantly. Conversely, reducing the pore size from 7 μm (Figure 10b) to 0.5 μm (Figure 10e) led to a significant reduction in the number of dots present. The highest concentration of dots observed is presented in Figure 10f, which was obtained at $T = 7.0$ °C, $P = 17.2$ bar, and $x_{CO_2}^* = 0.062$, and with 100 ppm of $KHCO_3$.

One explanation of these dots is that they were liquid water drops, formed as a result of the turbulent breakup of the liquid stream. However, the increase in dots at low temperatures, accompanied by a decrease in the amount of gas observed in the spray, suggests that additional phenomena were operative at low temperatures. For example, some of the dots may have been small dry ice particles or frozen water droplets, formed via Joule−Thomson cooling due to rapid expansion of CO_2 exiting the nozzle. Joule−Thomson expansion cooling has been applied previously to produce frozen microparticles from aqueous drops dispersed within supercritical CO_2, via ejection of the dispersion through a spray nozzle.[41] For these applications in which expansion cooling is desired, high nominal CO_2 mole fractions (0.5−0.9) are employed.[41] In our experiments, however, the nominal CO_2 mole fraction was typically <0.03. Hence, it is unlikely that a significant portion of the dots were formed via Joule−Thomson cooling, as large quantities of CO_2 were not present in the stream. An additional explanation of the dots involves CO_2 hydrate formation, which we consider in detail here.

The dot phenomenon trends observed in Figure 10 coincide with the improvement in spray pattern discussed in Sections 3.2, 3.4, and 3.5 and are consistent with the formation of CO_2 hydrate within the system. At ambient temperature, it is likely that dots present in the spray were liquid water drops,

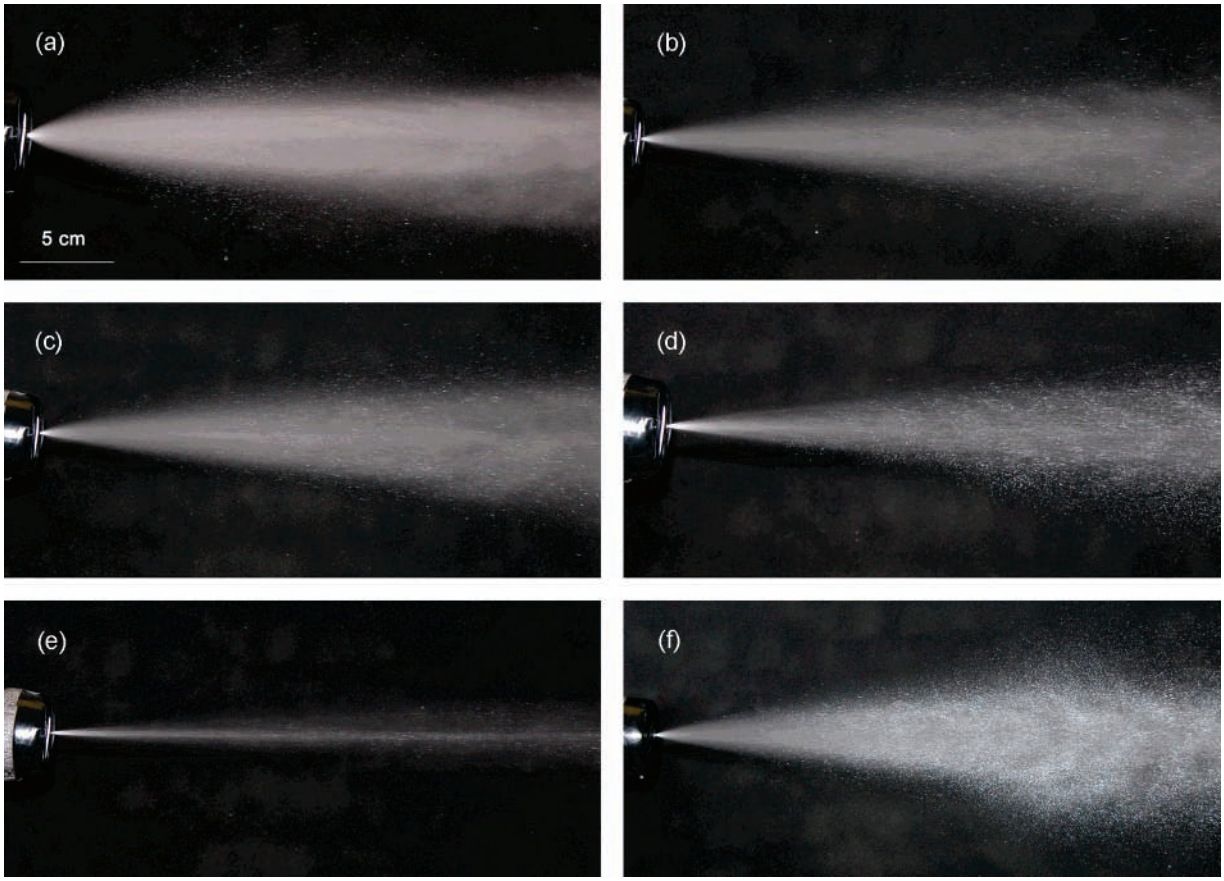

Figure 10. Images captured with camera flash on revealing dots in spray: (a) $x_{CO_2}^* = 0.025$, $T = 23$ °C, $P = 14.7$ MPa; (b) $x_{CO_2}^* = 0.026$, $T = 5$ °C, $P = 16.8$ MPa; (c) 100 ppm of $KHCO_3$, $x_{CO_2}^* = 0.025$, $T = 5$ °C, $P = 15.4$ MPa; (d) 100 ppm of SLS, $x_{CO_2}^* = 0.025$, $T = 6$ °C, $P = 14.2$ MPa; (e) 0.5 μm filter, $x_{CO_2}^* = 0.024$, $T = 6$ °C, $P = 14.4$ MPa; (f) 100 ppm of $KHCO_3$, $x_{CO_2}^* = 0.062$, $T = 7$ °C, $P = 17.2$ MPa.

formed by the shear imparted on the fluid as it rapidly depressurized through the nozzle. However, at low temperatures, hydrate formation is favorable on the surface of liquid CO_2 drops present in the system,[31,34−37] and some of these dots may have been hydrate-covered liquid CO_2 drops. For runs in which hydrate formation was enhanced, one would expect an increase in the number of dots observed due to an increase in the number of hydrate-coated CO_2 drops formed. Again, the formation of hydrate-coated CO_2 drops would have reduced the amount of CO_2 available to immediately expand upon exiting the nozzle.

Data sets 4 and 5 illustrate the consistency between spray divergence and dot formation. As shown in Figure 8, addition of 100 ppm of $KHCO_3$ did not reduce divergence of the spray, but divergence was reduced with 100 ppm of SLS. Accordingly, the number of dots observed in the spray was not affected by 100 ppm of $KHCO_3$, but increased with 100 ppm of SLS even though the divergence decreased (Figure 10). Additionally, inspection of Figure 10 reveals that less gas was visible in the 100 ppm SLS spray when compared to the 100 ppm $KHCO_3$ or additive-free sprays. This behavior is consistent with CO_2 being removed from the liquid phase (less divergence and visible gas) and being sequestered in the hydrate phase and within hydrate-coated CO_2 drops (increase in number of dots) for the 100 ppm SLS run.

Data sets 2 and 3 provide additional support for the interpretation of some dots as clathrate-containing particles. The reduction in filter size from 7 to 0.5 μm led to a reduction in spray divergence. In this case, the number of dots observed decreased. These observations are consistent with the removal of CO_2 from the liquid phase (less divergence) and into smaller hydrate-covered liquid CO_2 drops (decrease in number of observable dots). Smaller CO_2 drops, capable of forming smaller CO_2 hydrate-coated particles, would have been formed in this case because of the order-of-magnitude reduction in filter size.

3.8. Spontaneous Pressure Increase. The reduction in spray divergence that occurred at low system temperatures and in the presence of some additives suggests that CO_2 hydrate may have formed in our system. Further evidence for hydrate formation is provided by the behavior of the system pressure for some runs. In some experiments at low temperature and without additive, spontaneous pressure increases were observed after increasing the CO_2 flowrate from lower ($x_{CO_2}^* = 0.01$) to higher ($x_{CO_2}^* = 0.02$) flows. This interesting behavior is depicted in Figure 11, which demonstrates the effect of varying the CO_2 flowrate on the system pressure during an experiment at 4−5 °C without additive. For typical steady-state conditions, the system pressure was stable to within 0.1 MPa and did not change with time. This stable behavior is shown in interval A of Figure 11, where the CO_2 flowrate was 20 g/min ($x_{CO_2}^* = 0.009$) and the system pressure was 13.8 MPa. Increasing the CO_2 flowrate to 35 g/min ($x_{CO_2}^* = 0.018$) resulted in an increase in system pressure to 15.0 MPa, as shown in interval B. During interval B, the system pressure increased slowly to 15.5 MPa after roughly 4 min, although the CO_2 flowrate was held constant. Further increasing the CO_2 flowrate to 50 g/min ($x_{CO_2}^* = 0.026$, interval C) led to an immediate increase in system pressure to 16.5 MPa, which increased steadily for ∼12 s to 16.9 MPa. After this time, the pressure increased further, despite the CO_2 flowrate being held constant at 50 g/min, and it fluctuated wildly between 17 and 20 MPa, as the automatic shut-off feature of the H_2O pump was momentarily triggered at pressures >19

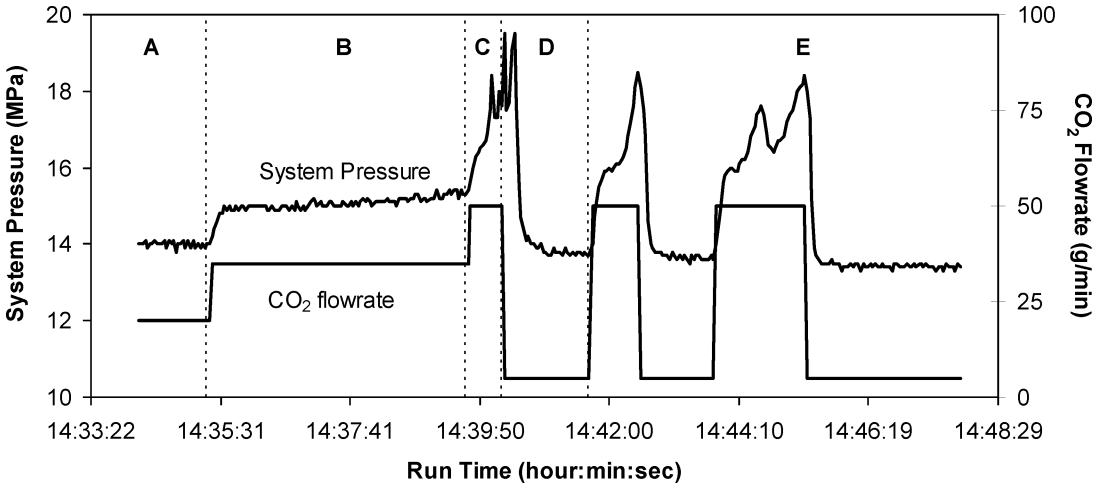

Figure 11. Spontaneous increases in system pressure with constant CO_2 flowrate: $x_{CO_2}^* = 0.026$, $T = 5$ °C.

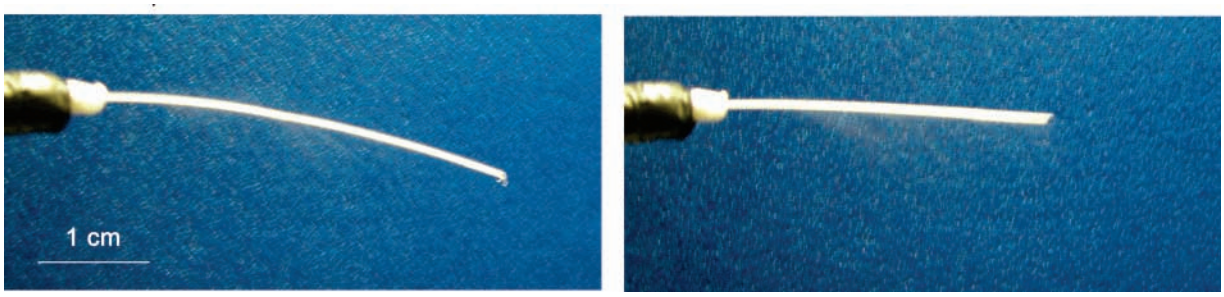

Figure 12. Hydrate-like substance observed during background experiments.

MPa. Lowering the CO_2 flowrate to only 5 g/min ($x_{CO_2}^* = 0.002$, interval D) quickly decreased the system pressure, which established a steady-state value of 13.8 MPa. Section E shows that the spontaneous pressure increase was reproducible and could be induced or ceased by increasing or decreasing the CO_2 flowrate, respectively.

The spontaneous pressure increases observed at constant CO_2 flowrate for H_2O-CO_2 flows at low temperature are consistent with precipitation of solid material in the system. Under these conditions, such solid particles may have been CO_2 hydrate, and hence, Figure 11 presents additional evidence for hydrate formation in the present experimental apparatus. Throughout interval B and during the first 12 s of interval C, the system pressure increased monotonically, even though the CO_2 flowrate was held constant. If these spontaneous pressure increases were due to the formation of hydrate, then the pressure should have increased more quickly during interval C, because the nominal CO_2 mole fraction and system pressure during interval C ($x_{CO_2}^* = 0.026$, $P = 16.5$ MPa) were both greater than those during interval B ($x_{CO_2}^* = 0.018$, $P = 15.0$ MPa). The greater availability of CO_2 and higher system pressure (greater hydrate-formation driving force) during interval C would have accelerated hydrate formation when compared to that during interval B. As shown in Figure 11, the pressure did increase more quickly during interval C than during interval B. These observations thus support the notion that CO_2 hydrate formed in the experimental high-pressure H_2O-CO_2 system.

The spontaneous pressure increases shown in Figure 11 demonstrate a potential for undesired plugging of the system, presumably because of uncontrolled formation of CO_2 hydrate. For the practical application of high-pressure, low-temperature H_2O-CO_2 sprays, it may be important to control system conditions so that plugging can be avoided. In the experiments conducted herein, plugging was not a significant problem when the system contained H_2O and CO_2, and further work is required to define the exact nature of this phenomenon.

3.9. Observation of a CO_2 Hydrate-like Substance. During background experiments conducted while developing the experimental apparatus, we observed the extrusion of a snow-like substance from the nozzle. Figure 12 displays this solid substance, which was opaque and white in color. This substance formed on two separate occasions, during which the system had clogged, flow out of the nozzle had ceased, and the contents of the system remained at high pressure for several seconds. Roughly 10 s after the clog occurred, the substance was slowly extruded from the nozzle at a velocity of ~3 cm s^{-1}. The length of the substance was maintained at roughly 3−4 cm, as the leading end of the substance broke away when the length of the substance exceeded this range. The substance slowly and steadily flowed out of the nozzle for ~30 s, after which time the solid was ejected from the nozzle by the pressurized fluid behind it and flow resumed.

One explanation of the solid substance is that it was simply ice that formed in the tubing. However, we expect that solid ice would have completely clogged the system and would have been ejected as a plug after partial thawing, rather than being expelled from the nozzle slowly and continuously as was the observed substance. This notion is supported by the fact that blockages, which occurred inadvertently when the system temperature was below 0 °C and only H_2O was present, were relieved in a catastrophic system depressurization. Furthermore, the substance shown in Figure 12 was never observed during an H_2O-only blockage. Thus, it is unlikely that the substance presented in Figure 12 is extruded ice.

The substance shown in Figure 12 formed when both H_2O and CO_2 were supplied to the system ($x_{CO_2}^* = 0.009$) and the system was at low temperature (0−10 °C) and high pressure ($P > 90$ bar). Hydrate formation was, hence, possible under

the conditions in which the substance formed. Furthermore, the substance presented in Figure 12 appears remarkably similar to CO_2 hydrate streams that have formed in other continuous systems. Lee et al.[5] and West et al.[6] synthesized a solid stream of CO_2 hydrate/liquid CO_2 composite using a coflow reactor similar to that used in the present work, wherein H_2O and liquid CO_2 were supplied to a length of tubing, mixed, and ejected from a nozzle. The similarity between their CO_2 hydrate composite and the solid substance presented in Figure 12 leads us to speculate that the substance did, in fact, contain CO_2 hydrate and was likely a CO_2 hydrate/H_2O composite because of the fact that the nominal CO_2 mole fraction (0.009) was less than the practical CO_2 mole fraction (0.115) of freshly formed CO_2 hydrate.[31] If all of the CO_2 present in the system was consumed in the form of hydrate, excess H_2O present may have served as a lubricant for extruding the compacted CO_2 hydrate particles, thereby facilitating flow of the hydrate/water composite.

The solid substance presented in Figure 12 could not be consistently reproduced, as a spontaneous and uncontrollable clog in the system precluded its formation on the two occasions in which it formed. However, we believe the summary of this phenomenon to be appropriate within the present discussion, where CO_2 hydrate formation is offered as an explanation for the improvement in spray pattern. Therefore, Figure 12 may provide visual evidence that hydrate formation was possible within the present experimental apparatus.

4. Summary and Conclusions

This experimental investigation demonstrated the concept of incorporating and delivering CO_2 within a high-pressure, low-temperature spray as a foaming agent for fire suppression without compromising the throw distance of the water jet. The effects of system temperature, filter pore size, additive, and nominal CO_2 mole fraction on the spray pattern of a high-pressure CO_2-H_2O stream ejected into the ambient environment were examined. Increasing the nominal CO_2 mole fraction induced a transition in the spray pattern from a compact liquid jet to a divergent spray. Significant reduction in the divergence of the spray was achieved by lowering the system temperature, reducing the in-line filter pore size (thereby increasing the mixing of the two streams and providing increased CO_2-H_2O interfacial contact), and adding 100 ppm of SLS or 100−3300 ppm levels of AFFF. The addition of 100 ppm of $KHCO_3$, however, had no effect on the spray pattern. These results provide useful guidelines for developing a practical method to enhance the fire-suppression capabilities of traditional H_2O/AFFF fire extinguishing systems.

Experimental observations suggest that CO_2 hydrate formed within the high-pressure apparatus and was ejected at the nozzle. The reductions in spray divergence at low (<10 °C) temperature, with added surfactant, and at decreased filter pore size are consistent with CO_2 being removed from the liquid phase and incorporated into a gas hydrate phase. The number of dots (small liquid droplets that may have contained or been coated with CO_2 hydrate) observed in spray images accordingly increased for runs, with the same filter size, in which the spray divergence decreased. A reduction in filter pore size led to a decrease in the concentration of observed dots, which is consistent with the production of smaller clathrate-containing particles. Additionally, spontaneous pressure increases (blockages) occurred when CO_2 was present within the system at temperatures above 0 °C. These observations collectively suggest that CO_2 within the system was effectively removed from the liquid phase and incorporated into a gas hydrate phase or within hydrate-covered liquid CO_2 droplets, which led to a reduction in spray divergence and, hence, improved the performance of the H_2O-CO_2 spray for fire-suppression applications.

Acknowledgment

The funding of this project by the Laboratory Director's Fund, Air Force Research Laboratory, Materials and Manufacturing Directorate, is gratefully acknowledged. The authors also would like to thank the following individuals for their support of this project in many ways: Dr. Glen Shen, Dr. Jean Renard, Virgil Carr, Robert Nichols, H. Scott MacLean, Carrie Delcomyn, Eric Mowles, Steven Wells, and Sue Broxson.

Literature Cited

(1) AFRL Success Stories, www.ml.afrl.af.mil/stories/mlq_asc_03_1721.html, 2003.

(2) Sloan, E. D. Clathrate Hydrates: The Other Common Solid Water Phase. *Ind. Eng. Chem. Res.* **2000**, *39*, 3123.

(3) Riestenberg, D.; Chiu, E.; Gborigi, M.; Liang, L.; West, O. R.; Tsouris, C. Investigation of Jet Breakup and Droplet size Distribution of Liquid CO_2 and Water Systems—Implications for CO_2 Hydrate Formation for Ocean Carbon Sequestration. *Am. Mineral.* **2004**, *89*, 1240.

(4) Tajima, H.; Yamasaki, A.; Kiyono, F.; Teng, H. New Method for Ocean Disposal of CO_2 by a Submerged Kenics-Type Static Mixer. *AIChE J.* **2004**, *50*, 871.

(5) Lee, S.; Liang, L.; Riestenberg, D.; West, O. R.; Tsouris, C.; Adams, E. CO_2 Hydrate Composite for Ocean Carbon Sequestration. *Environ. Sci. Technol.* **2003**, *37*, 3701.

(6) West, O. R.; Tsouris, C.; Lee, S.; McCallum, S. D.; Liang, L. Negatively Buoyant CO_2—Hydrate Composite for Ocean Carbon Sequestration. *AIChE J.* **2003**, *49*, 283.

(7) North, W. J.; Blackwell V. R.; Morgan, J. J. Studies of CO_2 Hydrate Formation and Dissolution. *Environ. Sci. Technol.* **1998**, *32*, 676.

(8) Sloan, E. D. Fundamental Principles and Applications of Natural Gas Hydrates. *Nature* **2003**, *426*, 353.

(9) Mao, W. L.; Mao, H. K. Hydrogen Storage in Molecular Compounds. *Proc. Natl. Acad. Sci. U.S.A.* **2004**, *101*, 708.

(10) Adisasmito, S.; Frank, R. J.; Sloan, E. D. Hydrates of Carbon Dioxide and Methane Mixtures. *J. Chem. Eng. Data* **1991**, *36*, 68.

(11) Bishnoi, P. R.; Natarajan, V. Formation and Decomposition of Gas Hydrates. *Fluid Phase Equilib.* **1996**, *117*, 168.

(12) Sloan, E. D. Introductory overview: Hydrate knowledge development. *Am. Mineral.* **2004**, *89*, 1155.

(13) Parent, J. S.; Bishnoi, P. R. Investigations into the Nucleation Behaviour of Methane Gas Hydrates. *Chem. Eng. Commun.* **1996**, *144*, 51.

(14) Uchida, T.; Ebinuma, T.; Kawabata, J.; Narita, H. Microscopic Observations of Formation Processes of Clathrate−Hydrate Films at an Interface between Water and Carbon Dioxide. *J. Cryst. Growth* **1999**, *204*, 348.

(15) Zatsepina, O. Y.; Riestenberg, D.; McCallum, S. D.; Gborigi, M.; Brandt, C.; Buffett, B. A.; Phelps, T. J. Influence of water thermal history and overpressure on CO_2—hydrate nucleation and morphology. *Am. Mineral.* **2004**, *89*, 1254.

(16) Zhong, Y.; Rogers, R. E. Surfactant Effects on Gas Hydrate Formation. *Chem. Eng. Sci.* **2000**, *55*, 4175.

(17) Lin, W.; Chen, G. J.; Sun, C. Y.; Guo, X. Q.; Wu, Z. K.; Liang, M. Y.; Chen, L. T.; Yang, L. Y. Effect of Surfactant on the Formation and Dissociation Kinetic Behavior of Methane Hydrate. *Chem. Eng. Sci.* **2004**, *59*, 4449.

(18) Zhang, C. S.; Fan, S. S.; Liang, D. Q.; Guo, K. H. Effect of Additives on Formation of Natural Gas Hydrate. *Fuel* **2004**, *83*, 2115.

(19) Song, Y.; Chen, B.; Nishio, M.; Akai, M. Measurement of Clathrate Hydrate Precipitation from CO_2 Solution by a Nondestructive Method. *Am. Mineral.* **2004**, *89*, 1247.

(20) Carstensen, A.; Creek, J. L.; Koh, C. A. Investigating the performance of clathrate hydrate inhibitors using in situ Raman spectroscopy and differential scanning calorimetry. *Am. Mineral.* **2004**, *89*, 1215.

(21) Dalmazzone, D.; Clausse, D.; Dalmazzone, C.; Herzhaft, B. The stability of methane hydrates in highly concentrated electrolyte solutions by differential scanning calorimetry and theoretical computation. *Am. Mineral.* **2004**, *89*, 1183.

(22) Zhang, Y.; Debenedetti, P. G.; Prud'homme, R. K.; Pethica, B. A. Differential Scanning Calorimetry Studies of Clathrate Hydrate Formation. *J. Phys. Chem. B* **2004**, *108*, 16717.

(23) Stern, L. A.; Kirby, S. H.; Circone, S.; Durham, W. B. Scanning electron microscopy investigations of laboratory-grown gas clathrate hydrates formed from melting ice, and comparison to natural hydrates. *Am. Mineral.* **2004**, *89*, 1162.

(24) Mork, M.; Schei, G.; Larsen, R. NMR Imaging Study of Hydrates in Sediments. In Gas Hydrates, Challenges for the Future; Holder, G. D., Bishnoi, P. R., Eds.; *Ann. N.Y. Acad. Sci.* **2000**, *912*, 897.

(25) Ratcliffe, C. I.; Ripmeester, J. A. ^{1}H and ^{13}C NMR Studies on Carbon Dioxide Hydrate. *J. Phys. Chem.* **1986**, *90*, 1259.

(26) Uchida, T.; Dallimore, S.; Mikami, J. Occurrences of Natural Gas Hydrates beneath the Permafrost Zone in Mackenzie Delta: Visual and X-ray CT Imagery. In Gas Hydrates, Challenges for the Future; Holder, G. D., Bishnoi, P. R., Eds.; *Ann. N.Y. Acad. Sci.* **2000**, *912*, 1021.

(27) Koh, C. A.; Savidge, J. L.; Tang, C. C. Time-Resolved in-Situ Experiments on the Crystallization of Natural Gas Hydrates. *J. Phys. Chem.* **1996**, *100*, 6412.

(28) Koh., C. A.; Westacott, R. E.; Zhang, W.; Hirachand, K.; Creek, J. L.; Soper, A. K. Mechanisms of gas hydrate formation and inhibition. *Fluid Phase Equilib.* **2002**, *194*−*197*, 143.

(29) Henning, R. W.; Schultz, A. J.; Thieu, V.; Halpern, Y. Neutron Diffraction Studies of CO_2 Clathrate Hydrate: Formation from Deuterated Ice. *J. Phys. Chem. A* **2000**, *104*, 5066.

(30) Someya, S.; Bando, S.; Chen, B.; Song, Y.; Nishio, M. Measurement of CO_2 Solubility in Pure Water and the Pressure Effect on it in the Presence of Clathrate Hydrate. *Int. J. Heat Mass Transfer* **2005**, *48*, 2503.

(31) Teng, H.; Yamasaki, A.; Shindo, Y. Stability of the Hydrate Layer Formed on the Surface of a CO_2 Droplet in High-Pressure, Low-Temperature Water. *Chem. Eng. Sci.* **1996**, *51*, 4979.

(32) Bozzo, A. T.; Chen, H. S.; Kass, J. R.; Barduhn, A. J. The Properties of the Hydrates of Chlorine and Carbon Dioxide. *Desalination* **1975**, *16*, 303.

(33) Uchida, T.; Ikeda, I. Y.; Takeya, S.; Ebinuma, T.; Nagao, J.; Narita, H. CO_2 hydrate film formation at the boundary between CO_2 and water: Effects of temperature, pressure and additives on the formation rate. *J. Cryst. Growth* **2002**, *237*−*239*, 383.

(34) Aya, I.; Yamane, K.; Yamada, N. Stability of Clathrate−Hydrate of Carbon Dioxide in Highly Pressurized Water. In *Fundamentals of Phase Change: Freezing, Melting, and Sublimation*; Kroeger, P. G., Bayazitoglu, Y., Eds.; ASME: Fairfield, NJ, 1992; pp 17−22.

(35) Shindo, Y.; Fujioka, Y.; Yanagisawa, Y.; Hakuta, T. Komiyama, H. Formation and stability of CO_2 hydrate. In *Direct Ocean Disposal of Carbon Dioxide*; Handa, N., Ohsumi, T., Eds.; TERRAPUB: Tokyo, 1995.

(36) Teng, H.; Kinoshita, C. M.; Masutani, S. M. Hydrate Formation on the Surface of a CO_2 Droplet in High-Pressure, Low-Temperature Water. *Chem. Eng. Sci.* **1995**, *50*, 559.

(37) Shindo, Y.; Lund, P. C.; Fujioka, Y.; Komiyama, H. Kinetics and Mechanism of the Formation of CO_2 Hydrate. *Int. J. Chem. Kinet.* **1993**, *25*, 777.

(38) Kang, S. P.; Lee, H.; Lee, C. S.; Sung, W. M. Hydrate Phase Equilibria of the Guest Mixtures Containing CO_2, N_2 and Tetrahydrofuran. *Fluid Phase Equilib.* **2001**, *185*, 101.

(39) Butler Ellis, M. C.; Tuck, C. R.; Miller, P. C. H. The effect of some adjuvants on sprays produced by agricultural flat fan nozzles. *Crop Prot.* **1997**, *16*, 41.

(40) Butler Ellis, M. C.; Tuck, C. R.; Miller, P. C. H. How surface tension of surfactant solutions influences the characteristics of sprays produced by hydraulic nozzles used for pesticide application. *Colloids Surf., A* **2001**, *180*, 267.

(41) Henczka, M.; Baldyga, J.; Shenkunov, B. Y. Modelling of spray-freezing with compressed carbon dioxide. *Chem. Eng. Sci.* **2006**, *61*, 2880.

Received for review April 26, 2006
Revised manuscript received July 18, 2006
Accepted August 1, 2006

IE060530P